



Simultaneous photocatalytic removal of nitrate and oxalic acid over Cu₂O/TiO₂ and Cu₂O/TiO₂-AC composites

Haruna Adamu^a, Alan J. McCue^a, Rebecca S.F. Taylor^b, Haresh G. Manyar^c, James A. Anderson^{a,*}

^a Surface Chemistry and Catalysis Group, Materials and Chemical Engineering, School of Engineering, University of Aberdeen, AB24 3UE, UK

^b School of Chemical Engineering and Analytical Science, The University of Manchester, The Mill, Sackville Street, Manchester, M13 9PL, UK

^c CentTACat, School of Chemistry and Chemical Engineering, Queen's University Belfast, David-Keir Building, Stranmillis road, Belfast, BT9 5AG, UK



ARTICLE INFO

Article history:

Received 24 February 2017

Received in revised form 29 May 2017

Accepted 30 May 2017

Available online 3 June 2017

Keywords:

Nitrate

Oxalic acid

Titania

Activated carbon

Composites

Photocatalysis

ABSTRACT

Cu₂O/TiO₂ (1–10 wt% Cu₂O) and 2.5% Cu₂O/TiO₂-AC (2.5–20 wt% AC) photocatalyst composites were synthesised by an ethanol reduction method. The materials were characterised by a number of techniques which confirmed the presence of Cu₂O in contact with the TiO₂. Pure TiO₂ alone was not active for the simultaneous photocatalytic removal of nitrate and oxalic acid under conditions employed, however, photocatalytic activity was observed for TiO₂ and TiO₂/AC in the presence of Cu₂O. This may have resulted from suppression of charge recombination via creation of a *p-n* heterojunction between Cu₂O and TiO₂. Within the series, 2.5% Cu₂O/TiO₂ exhibited the best photocatalytic performance with 57.6 and 99.8% removal of nitrate and oxalic acid, respectively, with selectivities of 45.7, 12.4 and 41.9% to NH₄⁺, NO₂⁻ and N₂, respectively after 3 h. For the carbon containing photocatalysts, 2.5% Cu₂O/TiO₂-2.5AC displayed the highest activity with 42.5 and 96.6% removal of nitrate and oxalic acid, respectively, with 32.7, 11.6 and 55.7% selectivities to NH₄⁺, NO₂⁻ and N₂, respectively. The highest AC loading tested resulted in selectivity to NH₄⁺ of 21.6 with no NO₂⁻ detected, together with an improved N₂ selectivity (78.4%) albeit at lower (12.7%) nitrate conversion. Data suggests that Cu₂O/TiO₂ can be used in the photocatalytic reduction of nitrate and improved selectivity towards N₂ can be attained by influencing factors which control the relative rate of oxalic acid consumption.

© 2017 Elsevier B.V. All rights reserved.

1. Introduction

Nitrate has become one of the most prevalent contaminants in groundwater, which originates from intensive agricultural activities, poor urban sewage management and waste disposal, as well as industrial effluents [1] and is seen as a serious global problem [2]. Organic pollutants are present in wastewater discharge from different industries including textiles, plastic, refinery, petrochemical, pharmaceutical, agrochemical and pulp and paper and may co-exist with nitrate [3,4]. Oxalic acid and other short organic acids are most likely to exist as intermediates following biological mineralisation of large organic molecules [3] and/or as one of incomplete mineralisation products of advanced oxidation treatments (AOT) [5].

Photocatalysis includes scope to simultaneously destroy residual organics and reduce inorganic ions such as nitrate from aqueous

solution [5] and are adjudged as a viable and promising technology for water pollution remediation [6]. TiO₂ is the most commonly explored photocatalyst although some studies indicate that TiO₂ is inactive for such a redox process [7,8], while others suggest either low activity [9] or high activity but with over-reduction of nitrate to ammonia [10,11]. Surface modification of TiO₂ with metals has been shown to be an effective manner of improving the efficiency of the photocatalytic reduction of nitrate in water [7,9,11–24] often by creation of Schottky barriers which act as sinks for photogenerated electrons. This consequently suppresses electron-hole recombination, as well as causing a negative shift in the Fermi level of the deposited metal [25,26], leading to increased reductive power.

Alternatively, a number of studies indicate that n-type TiO₂ combined with p-type metal oxide semiconductor may form a heterojunction which serves as an effective way of retarding recombination [27–30]. From research to date, n-type TiO₂ combined with p-type Cu₂O shows promise and uses a low-cost metal compared to others such as Ag [31,32]. This approach has been shown to be effective for diverse applications including degradation of organics [32–35] and the production of hydrogen [30,36,37]. It has

* Corresponding author.

E-mail address: j.anderson@abdn.ac.uk (J.A. Anderson).

been reported that p-type Cu₂O has a band gap of 2.0 eV [38] and a conduction band edge of −1.64 V [37]. Therefore, Cu₂O/TiO₂ can be exploited in the photocatalytic reduction of nitrate in the presence of organic hole scavengers, since the conduction band (CB) of TiO₂ is situated beneath that of Cu₂O and thus, electron-hole transfer between the heterojunction is thermodynamically permitted. Photogenerated electrons can move from Cu₂O to TiO₂ while holes migrate from the valence band (VB) of TiO₂ to Cu₂O, and as a result, the photodegradation mechanism of nitrate and oxalic acid over such composite differ from that of copper metal supported on TiO₂.

TiO₂ also suffers from an inherently low specific surface area and thus limited adsorption capacity because of crystallite growth during elevated calcination temperatures. Pre-adsorption of reactants, particularly the electron accepting species, on the photocatalyst surface is often deemed to be a prerequisite for rapid interfacial charge carrier trapping that leads to effective photochemical conversion [10]. It has been reported that coupling TiO₂ with activated carbon (AC) enhances photocatalytic degradation of pollutants because of increased adsorption capacity and improved interfacial charge transfer rate [39]. Such improvement in the photocatalytic efficiency of TiO₂/AC composites have been reported elsewhere [40–43]. In addition, the presence of activated carbon in TiO₂-AC composites may influence the photodegradation reaction pathway by generating different intermediate species compared to TiO₂ alone [44]. In this study, Cu₂O/TiO₂ and Cu₂O/TiO₂-AC photocatalyst composites were prepared and characterised and their ability to simultaneously photodegrade nitrate and oxalic acid assessed.

2. Experimental

2.1. Preparation of photocatalysts composites

All photocatalysts were prepared by an ethanol-based reduction method [30]. TiO₂ (Aeroxide P25, purchased from Sigma-Aldrich) was dispersed in anhydrous ethanol and stirred for 1 h before slow addition of the desired amount of Cu(NO₃)₂.3H₂O. After vigorous stirring for 2 h, the solvent was removed by drying at 60 °C for 6 h and the resultant sample was subsequently calcined at 350 °C for 2 h in air. The ethanol reduction method has been shown to produce materials with Cu loadings lower than the nominal values (more pronounced difference for higher loadings) [30]. Regardless, the as-prepared photocatalysts are denoted as x%Cu₂O/TiO₂, where x% represents nominal weight percent of loaded copper (1, 2.5, 5 or 10 wt%). Carbon containing Cu₂O/TiO₂-AC composites were prepared following the same method except that the desired amounts of activated carbon (AC) and TiO₂ were dispersed in anhydrous ethanol and stirred vigorously for 1 h before slow addition of the desired amount of Cu(NO₃)₂.3H₂O. The resulting composites were labelled as 2.5 Cu₂O/TiO₂-yAC (2.5 wt% was deemed to be the optimum copper loading – see later) where y reflects the loading of activated carbon (2.5, 5, 10 and 20 wt%) in the composites.

2.2. Photocatalysts characterisation

The X-ray diffraction pattern of the photocatalysts was examined using an X'Pert Pro Diffractometer (PANalytical) with a Cu Kα radiation source ($\lambda = 0.15418 \text{ nm}$) in the range 5–80° 2θ. Textural properties (surface area, pore volume and pore size) were determined by collecting N₂ adsorption-desorption isotherms at −196 °C on a Tristar-3000 instrument (Micromeritics). The optical properties of the photocatalysts were studied using a UV-vis spectrometer (Cary 60, Perkin-Elmer) in diffuse reflectance mode using a 60 mm diameter integrated sphere and BaSO₄ as the internal reference standard. To establish whether Cu influenced the band gap

of TiO₂ in the photocatalysts, plots of $(\alpha h\nu)^{1/2}$ versus E_{photon} was applied by fitting the absorption data to the equation. Reducibility of the copper component of the photocatalysts was investigated by temperature-programmed reduction (TPR) using a TPDRO 1100 instrument equipped with TCD detector. Samples were heated from 40 to 600 °C at 5 °C/min in a 5% H₂/N₂ mixture. The amount of hydrogen consumed was quantified based on a response factor determined using a CuO reference standard. The nature of exposed sites on the copper component was probed by studying the adsorption of CO by FTIR (Perkin-Elmer 1750 series spectrometer). The sample was pressed into a self-supporting disc and held in a quartz holder in a vacuum line which allowed for heating, evacuation and controlled gas manipulation. Samples were first outgassed and heated to 120 °C to remove surface water. The sample was then cooled to beam temperature and outgassed to a residual pressure of ca. $4 \times 10^{-5} \text{ Torr}$ before an initial spectrum (25 scans, 4 cm^{−1} resolution) was collected prior to exposure to increasing CO overpressures (0.3–40 Torr). Results are presented as difference spectra relative to the initial scan collected before exposure to CO.

XPS measurements were carried out using a Kratos AXIS Ultra DLD XPS spectrometer with monochromated AlKα X-rays and hemispherical analyser with a pass energy of 160 eV. The powdered samples were mounted on copper tape and binding energies were normalised to the C 1 s signal from adventitious carbon at 284.6 eV. Background subtraction was performed using a Shirley background and Casa XPS [45].

2.3. Photocatalytic tests

Photocatalytic reactions were carried out in a stirred, batch reactor fitted with a primary cooler (Fischer Scientific 3016S) to maintain the reaction temperature at 25 °C. A secondary cooling system was also incorporated to control heat given out by the 400 W UV lamp (Hereaus BQ 512 E, 400 W, 230 V and a maximum wavelength of 365 nm). Water was used as the coolant in this secondary cooling system by running a constant flow through a Pyrex cooler which encased the UV lamp. The Pyrex glass sleeve also functioned to filter out the light of wavelengths less than 290 nm which might otherwise lead to direct photolysis of nitrate and oxalic acid. Therefore, only light in the range between 290 and 365 nm were available for experiments conducted (Figure SI-1). In the experimental design, initially, 1.0 g/L photocatalyst composite was stirred in 1.5 L of ultra-pure water and N₂ bubbled for 30 min to displace dissolved oxygen. Thereafter, 100 mL stock solutions of nitrate (100 ppm) and optimal oxalic acid concentration (0.005 M) were added to the suspension. The reactor was stirred for another 1 h in the dark, which was determined to be beyond the minimum time required to ensure adsorption-desorption equilibrium was established. A sample was then taken to determine the equilibrium concentrations of the model pollutants in solution before the light was turned on ($t=0$). During the photocatalytic reaction test, samples were withdrawn with a 0.45 μm syringe filter at fixed time intervals over a 3 h reaction period. The net concentrations of nitrate and oxalate, as well as nitrite (one of the by-products of nitrate reduction), were measured using ion chromatography (Dionex DX-120), while ammonium was measured using a Merck Spectroquant ammonium test kit which follows the indophenol test for ammonium [46]. Thereafter, the degradation (%) of both model pollutants was calculated using Eq. (1).

$$\text{Degradation}(\%) = \frac{C_t}{C_0} \times 100 \quad (1)$$

where C₀ is the initial concentration at zero time, and C_t is the concentration after a particular period of illumination. The selec-

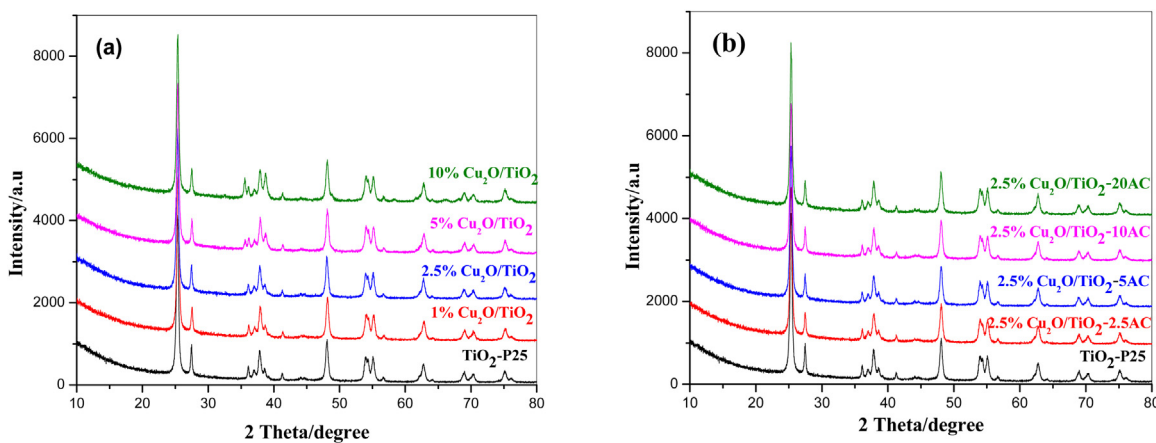


Fig. 1. XRD patterns of (a) Cu₂O/TiO₂ and (b) 2.5% Cu₂O/TiO₂-AC composites.

tivity toward N₂ (S_{N2}), NO₂⁻ (S_{NO2^-}) and NH₄⁺ (S_{NH4^+}) were defined according to Eqs. (2)–(4)) [21].

$$S_{(NH4^+)}\% = [NH4^+]_t / ([NO3^-]_0 - [NO3^-]_t) * 100 \quad (2)$$

$$S_{(NO2^-)}\% = [NO2^-]_t / ([NO3^-]_0 - [NO3^-]_t) * 100 \quad (3)$$

$$S_{(N2)}\% = ([NO3^-]_0 - [NO3^-]_t - [NH4^+]_t - [NO2^-]_t) / ([NO3^-]_0 - [NO3^-]_t) * 100 \quad (4)$$

where [X]₀ is the concentration at t = 0 and [x]_t is the concentration at time = t.

Metal loading was quantified before and after a photocatalytic test to access whether a Cu species was prone to leach under reaction conditions. Measurements were conducted by X-Ray fluorescence (XRF) using a Rigaku NEX QC+ instrument and indicated that the metal loading remained unchanged following use which confirms that leaching did not occur.

3. Results and discussion

3.1. Characterisation of photocatalysts

TG/DTG curves were obtained of the as-prepared samples prior to calcination at 350 °C. Heating was conducted from 25 to 350 °C in a flow of air. Samples with and without AC both showed similar profiles with mass loss occurring below 125 °C which can be attributed to loss of ethanol. No additional loss was detected for the AC containing samples or which increased as the loading of AC was increased which might otherwise be attributed to loss of carbon due to oxidation. This is consistent with previous results which reported that the onset of such a process was ca. 375 °C [47]. All subsequent characterisation is reported for materials following calcination at 350 °C.

The XRD patterns of all the materials are shown in Fig. 1. Intense peaks are apparent at 25.3, 37.9, 48.1, 54.0, 55.1, 62.8, 70.3 and 75.1° 2θ which correspond to the (101), (004), (200), (105), (211), (213), (202) and (215) crystal planes of the anatase phase of TiO₂, respectively (ICDD-01-075-2550). In addition, smaller features due to the rutile phase (ICDD-01-001-1292) were also detected (27.5, 36.2, 41.3, 56.7 and 69° 2θ). A weak peak was observed at 37.0° which is assigned to Cu₂O (111) crystallites (ICDD-01-077-7719), although this was only apparent for samples with greater than 2.5% Cu₂O loading. The titania crystallite sizes were calculated by application of the Scherrer equation and are displayed in Table 1. Pure TiO₂ has a crystallite size of 42.5 nm and the addition of Cu and activated car-

bon caused no significant change in the crystallite size, irrespective of the loadings.

Nitrogen adsorption-desorption isotherms of all materials were collected in order to understand the impact of the composition on the textural properties (Table 1). The surface area of TiO₂ progressively decreased with increasing Cu loading, however, incorporation of activated carbon into the composite at fixed copper loading (2.5% Cu₂O/TiO₂) resulted in a gradual increase in the surface area. The nitrogen adsorption-desorption isotherms (not shown) all exhibited type IV hysteresis loops characteristic of mesoporous solids. Incorporation of Cu₂O resulted in a larger average pore size and a corresponding increase in pore volume.

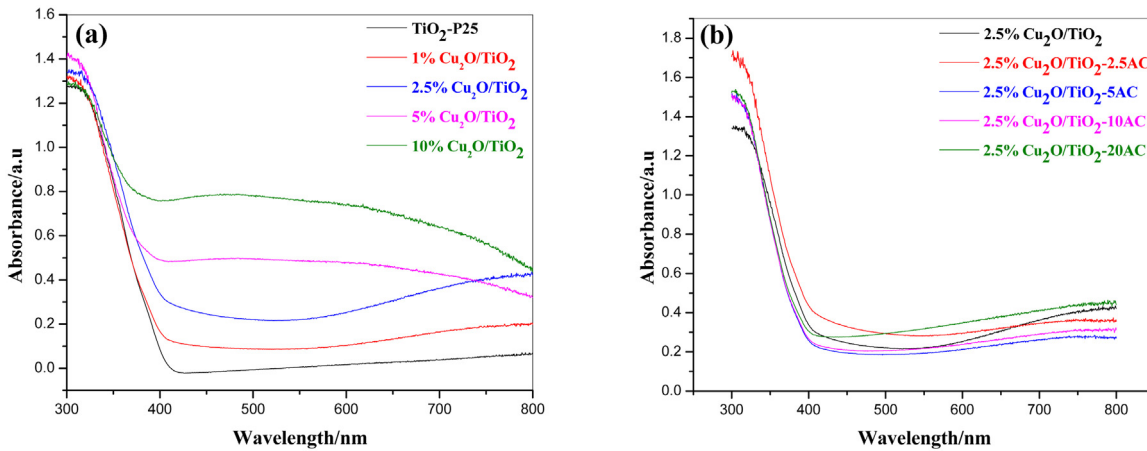
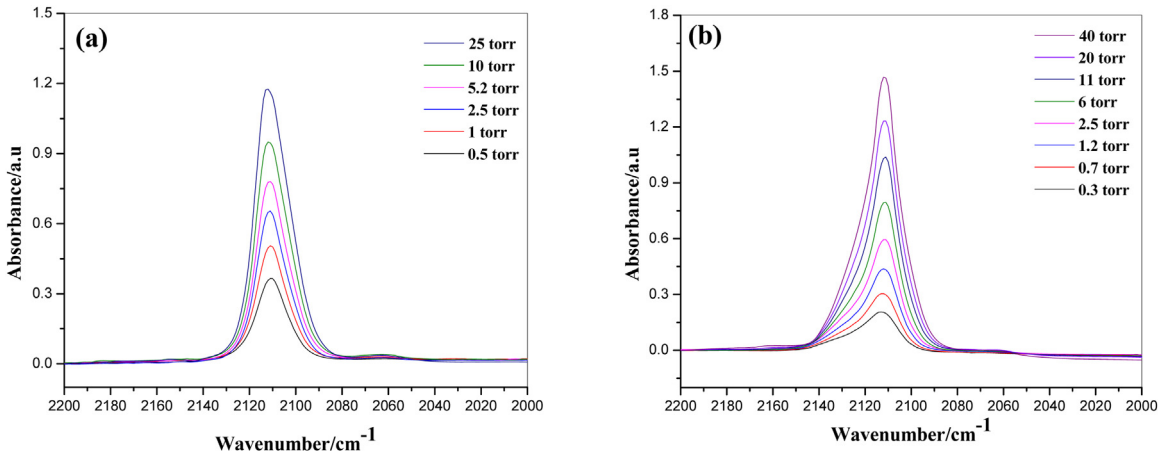
The UV-vis spectra of samples are shown in Fig. 2. All of the Cu₂O/TiO₂ samples exhibit an increase in absorption at wavelengths longer than 400 nm compared to the absorption edge of pure TiO₂. Such a shift towards the visible region can be related to an electronic transition involving Cu, as is contained in the Cu₂O/TiO₂ composite photocatalysts. The band gap exhibited by the Cu₂O/TiO₂ composites was narrowed as identified by increased absorption towards visible light range and, additionally showed decreased band gap with increasing Cu₂O in the composites (Table 1 and Fig. 2a). Amongst the carbon containing composites, 2.5% Cu₂O/TiO₂-2.5AC absorbed light at wavelengths longer than its corresponding composite in the absence of activated carbon (Fig. 2b). The shift towards the visible light region in the 2.5% Cu₂O/TiO₂-2.5AC composite signifies further decrease in band gap as compared to 2.5% Cu₂O/TiO₂ (Table 1), which may potentially be associated with incorporation of carbon into the TiO₂ structure. However, examination of the UV-vis spectra of samples with higher loadings of activated carbon beyond 2.5 wt% was a challenge. Despite these difficulties, it was noted that composites with activated carbon loadings above 2.5% showed similar absorption edge positions (and band gaps) as 2.5% Cu₂O/TiO₂ (not shown here). This could be interpreted as a result of the activated carbon presenting a light shielding effect on the Cu₂O/TiO₂ component, as no further impact (comparing with the sample of 2.5% Cu₂O/TiO₂) on the electronic transition was observed for samples containing greater than 2.5 wt% activated carbon.

FTIR spectroscopy of adsorbed CO was employed to extract information regarding the exposed surfaces of the copper component in the samples. CO adsorbed onto exposed Cu²⁺ sites shows a band at 2200 cm⁻¹ whereas peaks indicative of Cu⁺ species and Cu⁰⁰ generally appear at 2102–2133 and 2060–2080 cm⁻¹, respectively [48–53]. Fig. 3a and b show the spectra of adsorbed CO on 1% and 2.5% Cu₂O/TiO₂ samples, respectively. The main absorption band for both samples appeared at 2110 cm⁻¹ and is attributed to CO adsorption on Cu⁺, consistent with the presence of Cu₂O. A

Table 1

Physical properties of the materials.

Materials	S_{BET} (m^2/g)	Pore volume (cm^3/g)	Average pore size (nm)	XRD crystallite size (nm)	Band gap (eV)
Pure TiO_2 -P25	52	0.21	16.2	42.5	3.2
1% $\text{Cu}_2\text{O}/\text{TiO}_2$	51	0.40	27.9	41.3	3.12
2.5% $\text{Cu}_2\text{O}/\text{TiO}_2$	50	0.38	26.7	42.0	3.0
5% $\text{Cu}_2\text{O}/\text{TiO}_2$	49	0.39	26.9	41.2	2.95
10% $\text{Cu}_2\text{O}/\text{TiO}_2$	46	0.38	28.5	41.2	2.85
2.5% $\text{Cu}_2\text{O}/\text{TiO}_2$ -2.5AC	51	0.41	27.5	41.8	2.90
2.5% $\text{Cu}_2\text{O}/\text{TiO}_2$ -5AC	53	0.40	27.6	42.7	3.05
2.5% $\text{Cu}_2\text{O}/\text{TiO}_2$ -10AC	55	0.37	25.1	41.4	3.05
2.5% $\text{Cu}_2\text{O}/\text{TiO}_2$ -20AC	96	0.38	19.3	41.9	3.05

**Fig. 2.** UV-vis diffuse reflectance spectra of (a) $\text{Cu}_2\text{O}/\text{TiO}_2$ and (b) 2.5% $\text{Cu}_2\text{O}/\text{TiO}_2$ -AC composites.**Fig. 3.** FTIR spectra of CO adsorbed on (a) 1% $\text{Cu}_2\text{O}/\text{TiO}_2$ and (b) 2.5% $\text{Cu}_2\text{O}/\text{TiO}_2$.

small band is observed at *ca* 2060 cm⁻¹ confirming the presence of a small population of Cu^0 sites. Note however that the absorption coefficient of CO on Cu^+ is known to be greater than for CO on Cu^0 [49] meaning that the Cu^0 population is likely to be even lower than observed qualitatively. No samples exhibited a peak which could be assigned to CO adsorbed on Cu^{2+} .

In order to evaluate the reducibility of copper species, H₂-TPR profiles were collected (Fig. 4). Both 1 and 2.5% $\text{Cu}_2\text{O}/\text{TiO}_2$ display a sharp reduction peak at *ca.* 160 °C, although 2.5% $\text{Cu}_2\text{O}/\text{TiO}_2$ also gave another broad reduction peak at *ca.* 225 °C. Reduction of $\text{Cu}^+ \rightarrow \text{Cu}^0$ must occur in a single step whereas reduction of $\text{Cu}^{2+} \rightarrow \text{Cu}^0$ can occur *via* a two-step process. However, no evidence of a Cu^{2+} species was observed by FTIR (Fig. 3). As such, the reduction peak at *ca.* 160 °C is assigned to Cu_2O species that are readily reduced due to their high dispersion on the support, while the addi-

tional peak centred at *ca.* 225 °C for 2.5% $\text{Cu}_2\text{O}/\text{TiO}_2$, could be related to reduction of Cu_2O species that are weakly interacted with the support and/or with a larger particle size [50,54]. Incorporation of AC in the metal oxide composite shifted the main reduction peak to *ca.* 190 °C, along with a more pronounced second peak at *ca.* 300 °C. The broadness of the other peak perhaps resulted from the nature of the interaction of Cu_2O species with the supports (i.e., TiO_2 -AC), in which some of Cu_2O species are either loosely held or have no interaction with the support [50]. No peak was observed which could be attributed to the reduction of surface oxygen containing functionalities on the activated carbon, although it is possible that such features existed above 600 °C [55]. The percentage reduction was estimated from the consumption of hydrogen and the results are shown in Table 2. All samples exhibited less than 50% Cu reduction (on the basis of Cu^{2+} as starting material) providing further

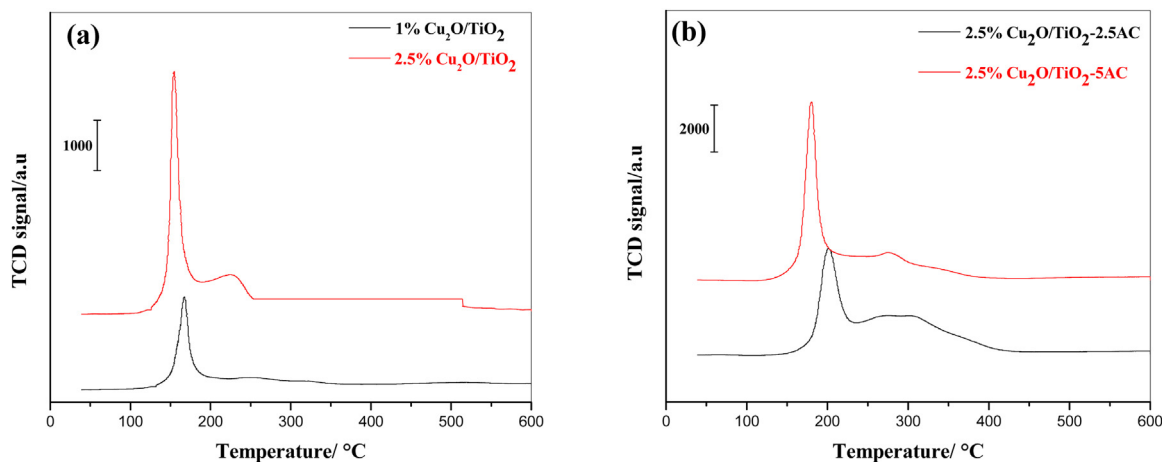


Fig. 4. TPR profiles of (a) 1 and 2.5% Cu₂O/TiO₂, and (b) 2.5% Cu₂O/TiO₂-2.5AC and 2.5% Cu₂O/TiO₂-5AC.

Table 2
Degree of reduction of the copper phase in photocatalysts.

Materials	Extent of Cu reduction (%)
1% Cu ₂ O/TiO ₂	18.4
2.5% Cu ₂ O/TiO ₂	30.3
2.5% Cu ₂ O/TiO ₂ -2.5AC	30.9
2.5% Cu ₂ O/TiO ₂ -5AC	33.8

evidence for the absence of Cu²⁺ in the initial samples. All samples consumed less hydrogen than required to stoichiometrically reduce Cu₂O which suggests that at least some of the copper may have initially been present in a reduced form, consistent with the FTIR results (Fig. 3).

XPS analyses were conducted to gain insight into the nature of Cu ions in the two types of support. XPS spectra of Cu 2p core level profiles of 1% Cu₂O/TiO₂, 2.5% Cu₂O/TiO₂ and 2.5% Cu₂O/TiO₂-2.5AC are displayed in Fig. 5a–c, respectively. The Cu 2p_{3/2} characteristic peaks Cu⁰, Cu₂O, and CuO appear at 932, 932.7 and 933.6 eV [36], respectively. The Cu 2p_{3/2} and 2p_{1/2} binding energy values for 1% Cu₂O/TiO₂ appeared at 931.5 and 951.5 eV, confirming the presence of Cu⁺ in 1% Cu₂O/TiO₂ (Fig. 5a). The Cu nanoparticles were present as Cu₂O rather than Cu⁰ or CuO as Cu⁺ (Cu₂O) does not exhibit Cu 2p satellite peaks since the 3d band of Cu₂O is filled (3d¹⁰) and the 4s band is unoccupied [56]. However, in the 2.5% Cu₂O/TiO₂ and 2.5% Cu₂O/TiO₂-2.5AC, apart from the Cu 2p_{3/2} and 2p_{1/2} characteristic peaks of Cu⁺, high energy satellite structures are found between 936 and 943 eV, which are associated with Cu²⁺ species. This weak satellite peak found in the samples of 2.5% Cu₂O/TiO₂ and 2.5% Cu₂O/TiO₂-2.5AC establishes that small quantities of Cu²⁺ are present, and thus exist in the process of Cu₂O nanoparticle formation on the surface of TiO₂ and TiO₂-AC supports. Therefore, these samples may be compared with data for the reduction of nitrate in presence of oxalic acid for previous copper based photocatalysts where Cu existed predominantly in a zero or plus two oxidation state [7,8,10,16,24,57].

3.2. Photocatalytic removal of nitrate and oxalic acid over Cu₂O/TiO₂

The photocatalytic activities of the photocatalyst composites were evaluated in the simultaneous removal of nitrate and oxalic acid under UV irradiation with results summarised in Table 3. Under the condition employed, pure TiO₂ was found to be inactive in the photocatalytic reduction of nitrate, consistent with some previous observations [7,8] although did degrade oxalic acid to some extent. Under similar conditions, copper oxide on silica showed no

photocatalytic activity. For the composite oxides based on titania, increasing the Cu₂O loading resulted in faster degradation of the oxalic acid. Nitrate reduction was also apparent, although a limiting maximum conversion was reached once the hole scavenger was fully consumed (i.e., nitrate conversion reached a plateau). The rate of both nitrate reduction and oxalic acid oxidation can be described by apparent first order kinetics (Fig. 6a–b). Maximum nitrate conversion was obtained over 2.5% Cu₂O/TiO₂ (Fig. 6c), although N₂ and NH₄⁺ were produced in almost equal quantities, with relatively little tendency to form nitrite. Higher Cu₂O loadings resulted in faster oxalic acid degradation, lower nitrate conversion and an increased tendency to form ammonium. As such, 2.5% was chosen as the optimum Cu₂O loading for the preparation of carbon containing composites. Results presented here indicate that addition of Cu₂O enhanced the photocatalytic potential of TiO₂ for the reduction of nitrate, presumably via effective charge carrier separation. It has been reported that Cu₂O has poor stability in aqueous solutions, because the redox potentials for the reduction and oxidation of monovalent copper oxide lie within the bandgap [58] and thus, is quite limiting in terms of its application in aqueous solutions. However, combining Cu₂O with TiO₂ is a potential solution to the problem of the instability of Cu₂O in water under illumination. As TiO₂ serves as a protective n-type oxide, whose conduction band lies in between the Cu₂O valence and conduction band positions and therefore, it assists in extracting photogenerated electrons from Cu₂O leading to improve the stability of Cu₂O in water under illumination (i.e., avoiding the reduction of Cu₂O to Cu). Hence, the photocatalytic nitrate reduction mechanism involving Cu₂O/TiO₂ is most likely different from M/TiO₂ (M = metallic Ag, Cu, Fe, etc.), in which case M/TiO₂ is a semiconductor-metal contact that improves such reaction by the ability of the metal to localise the photogenerated electrons and thus become the site for the reduction process. In the coupled Cu₂O/TiO₂ system, TiO₂ lies below the conduction band edge of Cu₂O thereby acting as an electron sink by mediating electrons away from Cu₂O, while Cu₂O is above the valence band edge of TiO₂ trapping the holes formed. This electron-hole pair movement creates a scenario where Cu₂O will be left with more holes, whereas TiO₂ will exist with high density of electrons that will heighten its conduction band and thus becomes reductive enough. Consequently, the photodegradation mechanism of oxalic acid and nitrate over such composite is different from the conventional mechanistic approach in the same reaction using Cu/TiO₂ system.

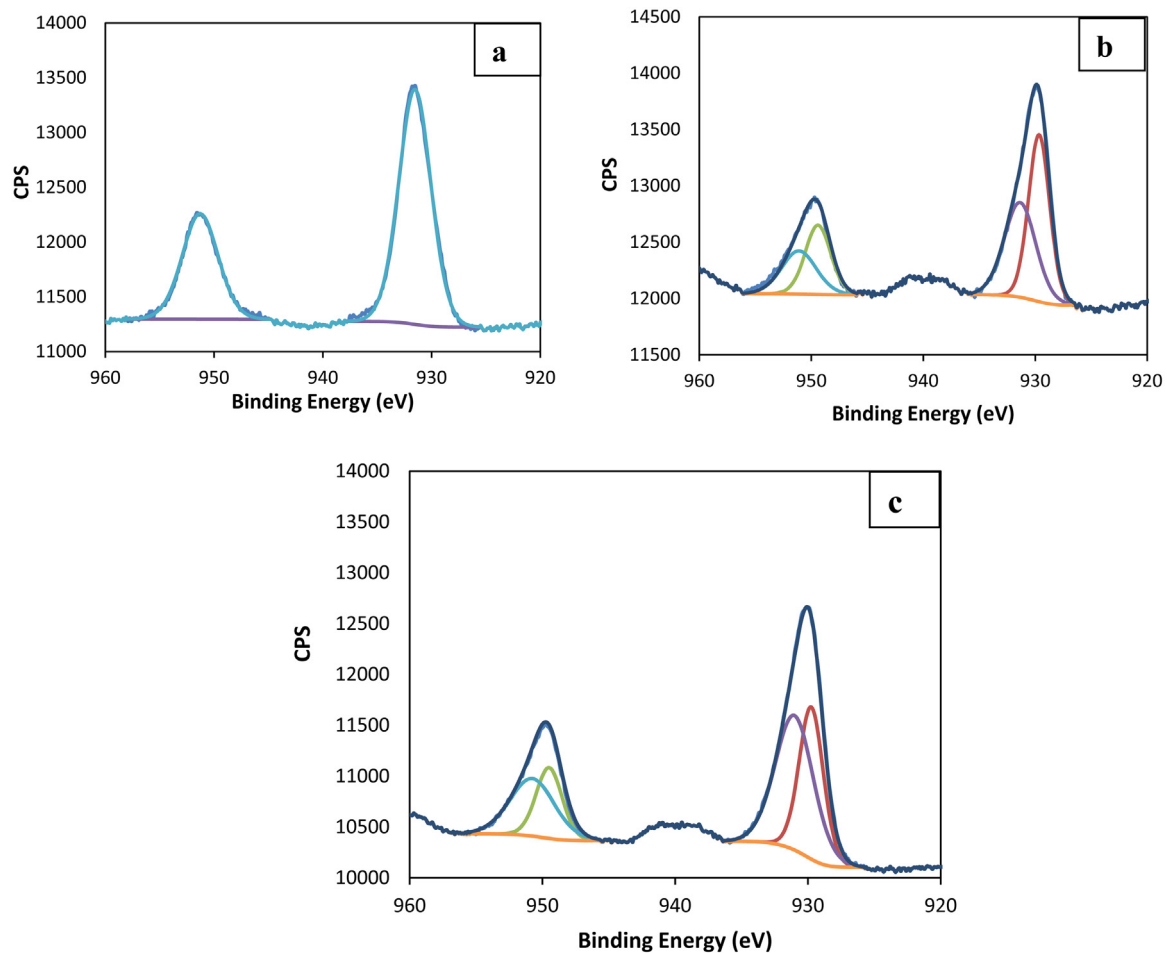


Fig. 5. XP Spectra of (a) 1% Cu₂O/TiO₂, and (b) 2.5% Cu₂O/TiO₂ and (c) 2.5% Cu₂O/TiO₂-2.5AC.

Table 3

Conversion, rate constants (k), and selectivities for TiO₂ and Cu₂O/TiO₂ photocatalysts.

Materials	Nitrate conversion (%)	Oxalate conversion (%)	Rate constant, k (min ⁻¹)			
				Nitrate	Oxalate	NH ₄ ⁺ selectivity (%)
TiO ₂ -P25	0	31	0	0.0027	0	0
1% Cu ₂ O/TiO ₂	40.4	94.1	0.0036	0.0143	36.5	14.6
2.5% Cu ₂ O/TiO ₂	57.6	99.8	0.0058	0.0166	45.7	12.4
5% Cu ₂ O/TiO ₂	31.2	98.4	0.0023	0.0174	59.2	11.7
10% Cu ₂ O/TiO ₂	28.3	100	0.0014	0.0198	64.6	9.2

3.2.1. Influence of initial oxalic acid concentration

Oxalic acid concentration is known to influence photocatalytic performance as the oxalate anion may compete with nitrate for adsorption sites [8]. At low solution concentration of oxalic acid, the amount adsorbed is limited and although it has less impact on nitrate adsorption, it is unable to effectively trap holes and as a result, nitrate reduction is limited. At high concentrations, oxalic acid is adsorbed with high surface coverage which limits nitrate coverage and hence lowers the conversion of the latter [8]. Consequently, it is important to determine the appropriate concentration of oxalic acid for effective nitrate conversion. Due to the known preferential adsorption of oxalic acid over nitrate, oxalic acid concentrations of 0.005 [7,8,10] and 0.008 M [24] as previously reported were tested to allow direct comparison with literature data. When using 0.008 M oxalic acid, 8.5 mol of oxalic acid were consumed per mole of nitrate (Fig. 7a), fairly consistent with previous reports under equivalent conditions [24]. This

value decreased to 5.4 when the initial oxalic acid concentration was reduced to 0.005 M (Fig. 7a), which implies a more effective use of hole scavenger and suggests that nitrate can successfully compete with oxalic acid for adsorption sites at this concentration. Therefore, the remainder of tests described here make use of 0.005 M oxalic acid. The experimental value of 5.4 is still approximately 2 times higher than the stoichiometric value (Eq. (5)) in a reaction involving 5 and 2 electrons for nitrate reduction and oxalic acid oxidation, respectively. However, lowering of the concentration further to 0.004 M has been reported [24] to bring the experimental relationship closer to the theoretical stoichiometry.

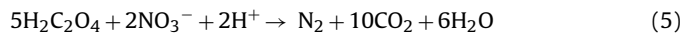


Fig. 7b displays the apparent rate constants for removal of both oxalic acid and nitrate as functions of the initial oxalic acid to nitrate molar ratio at a fixed initial nitrate concentration (100 ppm, 0.0016 M). Nitrate removal was achieved at each oxalic acid-nitrate

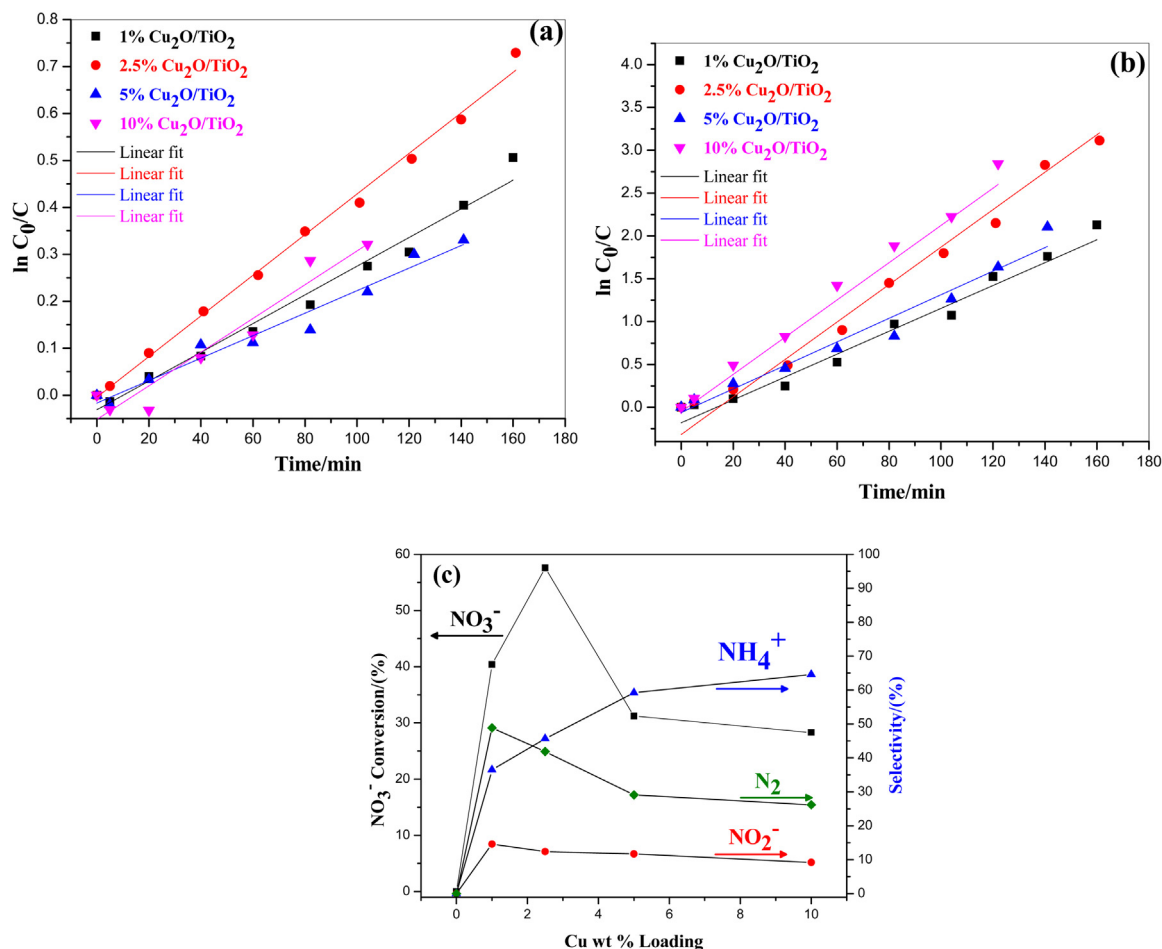


Fig. 6. Apparent first order plots based on simultaneous nitrate/oxalic acid removal for (a) nitrate reduction and (b) oxalic acid oxidation and (c) final (3 h) nitrate conversion and product selectivity as a function of Cu₂O loading.

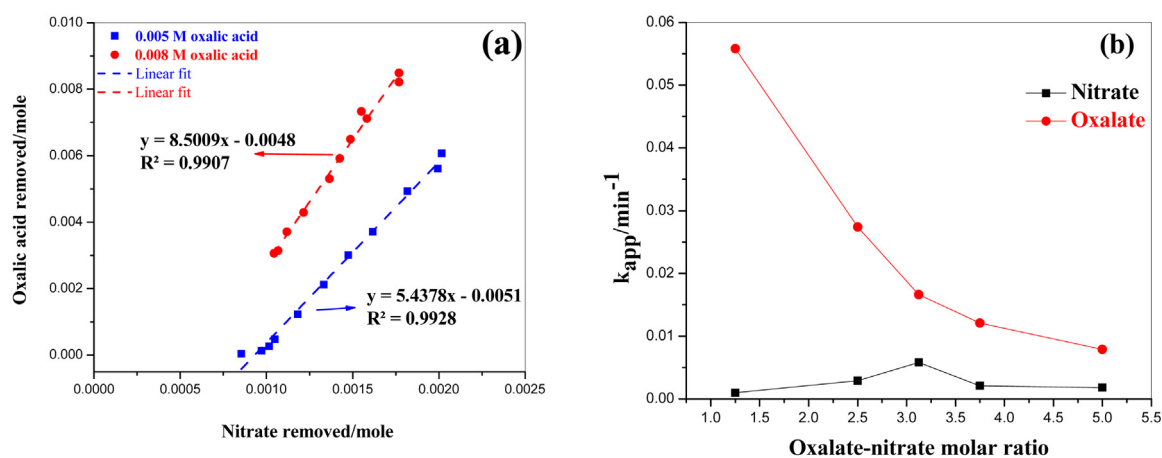


Fig. 7. (a) Relationship between extent of oxalic acid nitrate removal over 2.5% Cu₂O/TiO₂, (b) rate constants for oxalic acid and nitrate as a function of oxalic acid-nitrate molar ratio at a constant initial nitrate concentration 100 ppm (0.0016 M).

molar ratio, however, increased oxalic acid-nitrate molar ratio did not result in significant improvement. A minimum rate constant was attained for an oxalic acid-nitrate molar ratio of 1.3 and a maximum at 3.1.

3.2.2. Dependence of mass of photocatalyst

The mass of photocatalysts is a key parameter that controls the rate of degradation of pollutants with the rate expected to

increase proportionally with increasing mass until a maximum limit is reached [59]. In this study, the optimum mass of 2.5% Cu₂O/TiO₂ was investigated within the range 0.25–2.0 g/L (Fig. 8). Rate of consumption of both pollutants increased linearly up to 1 g L⁻¹ where maximum rate constants of 0.0058 and 0.0166 min⁻¹ for nitrate and oxalic acid, respectively, were obtained. Above this value, a decrease in rate was observed, presumably as a result of shielding and scattering of radiation. Above a limiting mass of pho-

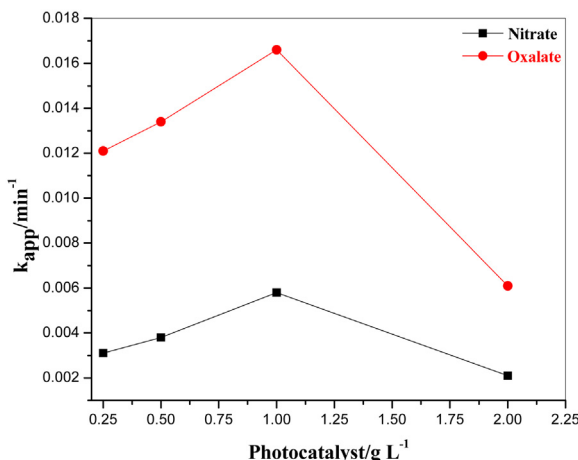


Fig. 8. The effect of mass of 2.5% $\text{Cu}_2\text{O}/\text{TiO}_2$ photocatalyst on the rates of nitrate and oxalic acid removal.

tocatalyst, the turbidity of the reaction solution increases which impedes the penetration of UV light [60].

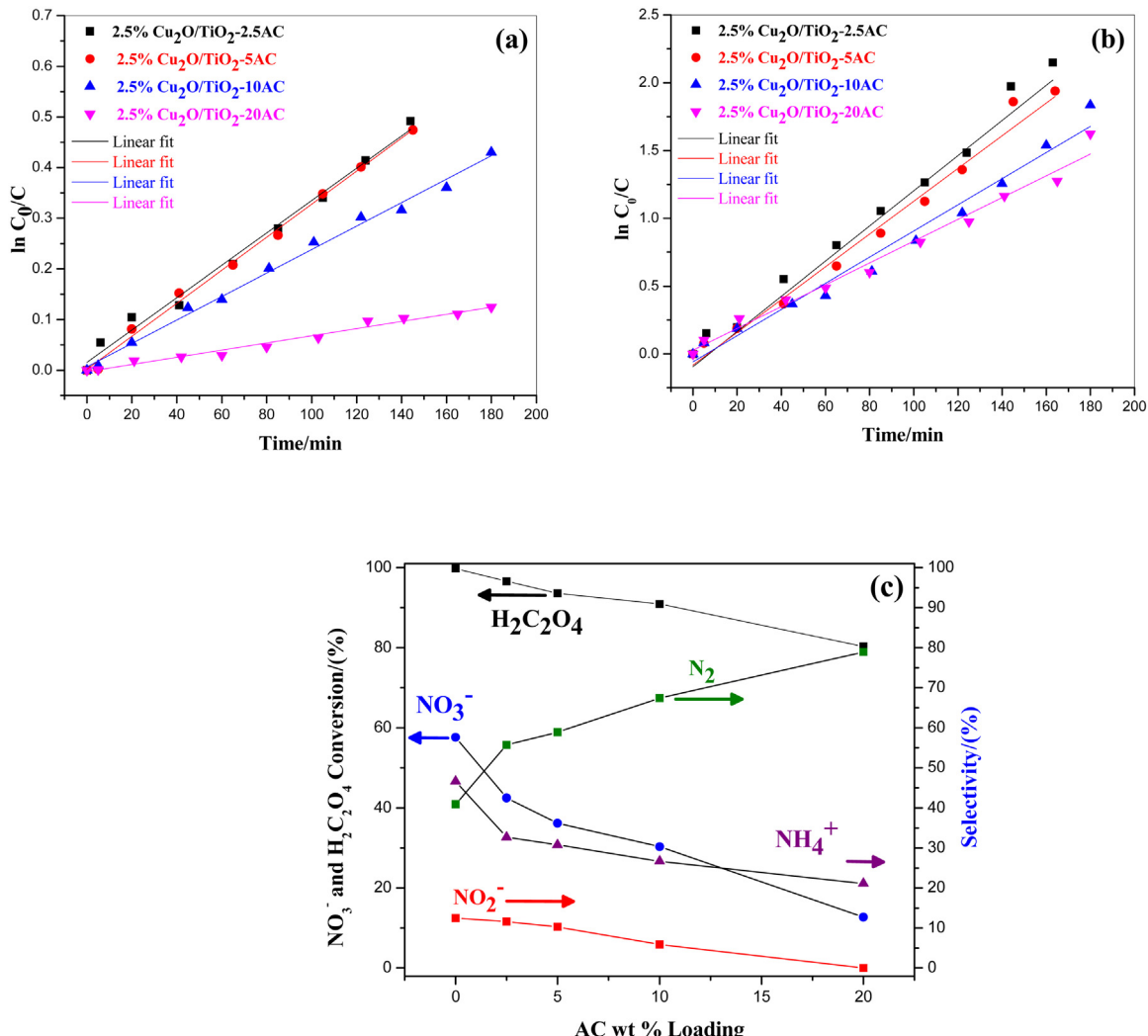


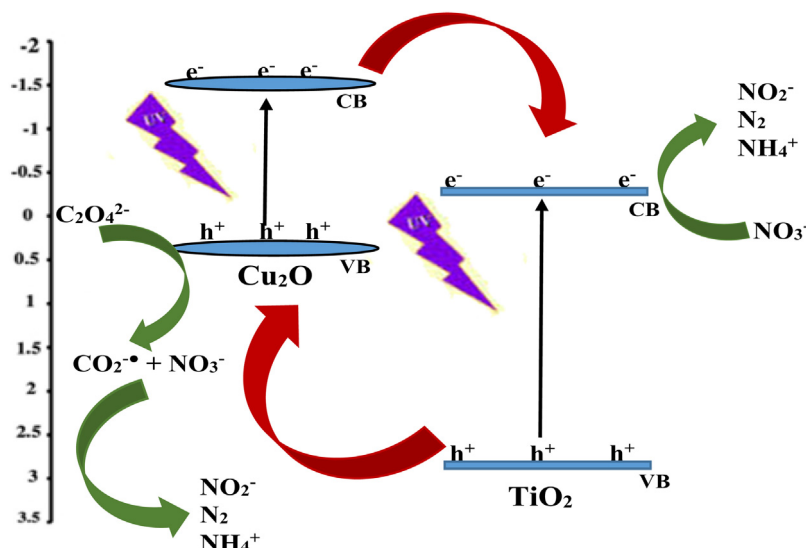
Fig. 9. Apparent first order plots for (a) nitrate reduction and (b) oxalic acid oxidation. (c) oxalic acid/nitrate conversion and product selectivity as a function of AC loading.

3.3. Photocatalytic removal of nitrate and oxalic acid over $\text{Cu}_2\text{O}/\text{TiO}_2$ -AC

Fig. 9 displays the photocatalytic performance of 2.5% $\text{Cu}_2\text{O}/\text{TiO}_2$ -AC composites and reveals that the addition of increasing amounts of AC decreased both oxalic acid and nitrate conversion. This may in part be associated with light shielding/scattering by the AC as reported elsewhere [61,62]. The rate of nitrate reduction and oxalic acid oxidation were still best described by an apparent first order expression (**Fig. 9a** and b). Increasing the AC content led to increased nitrogen selectivity and decreased ammonium and nitrite selectivity. The overall yield to nitrogen remained roughly constant at ca 23% due to the inverse trend between nitrate conversion and nitrogen formation. This seems to be governed by the slower rate of oxalic acid conversion (see Figure SI-3 and compare to SI-2). Therefore, the incorporation AC with $\text{Cu}_2\text{O}/\text{TiO}_2$ reduced the reaction rates, (i.e. reduced the quantum efficiency) but was advantageous in terms of nitrogen selectivity.

3.4. Photocatalytic nitrate reduction mechanism

The mechanism involved in the use of composite p-type and n-type semiconductor photocatalyst is different from the Cu/TiO_2 [63] system in which Cu ions are deposited and subsequently reduced. In the materials described here, TiO_2 is coupled with p-type Cu_2O



Scheme 1. Proposed mechanism for the simultaneous photocatalytic removal of nitrate and oxalic acid over $\text{Cu}_2\text{O}/\text{TiO}_2$ photocatalyst.

semiconductor, meaning that under UV-vis illumination, photo-generated electrons can be transferred from the conduction band of Cu_2O to TiO_2 and holes migrate from the valence band of TiO_2 to Cu_2O , as a result of matched band structure between the two semiconductors [27,30]. This type of photogenerated electron-hole pair transfer between p-type Ag_2O and TiO_2 -P25 has been reported recently [63]. This implies that both Cu_2O and TiO_2 can be simultaneously photoactivated and generate electron-hole pairs in accordance with Eqs. (6) and (7), as;

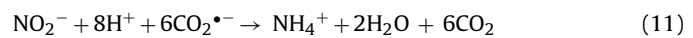
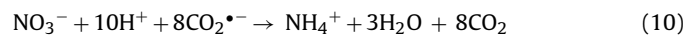
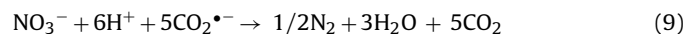


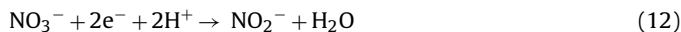
This is followed by the consumption of photogenerated electrons and holes by adsorbed nitrate and oxalic acid, respectively, as illustrated in Scheme 1. Previous investigations [7,8,10] have reported that reduction of nitrate in the presence of the oxalate anion proceeded indirectly via formation of an oxalate radical which decomposed to produce $\text{CO}_2\bullet^-$ (Eq. (8)). It has been shown that $\text{CO}_2\bullet^-$ -species have strong reductive ability ($E^\circ(\text{CO}_2/\text{CO}_2\bullet^-) = -1.8 \text{ V}$) [10], capable of reducing nitrate to N_2 ($E^\circ(\text{NO}_3^-/\text{N}_2) = 1.25 \text{ V}$) (Eq. (8)) or to ammonium ($E^\circ(\text{NO}_3^-/\text{NH}_4^+) = 1.203 \text{ V}$; ($E^\circ(\text{NO}_2^-/\text{NH}_4^+) = 0.897 \text{ V}$) (Eqs. (10) and (11)) [7–9]. The reduction of nitrite to N_2 ($E^\circ(\text{NO}_2^-/\text{N}_2) = 1.45 \text{ V}$) was not possible in all the reactions carried out with $\text{Cu}_2\text{O}/\text{TiO}_2$ systems, as the formation of ammonium in the reactions was continuously built up while nitrite generation and nitrogen selectivity were diminished concomitantly (Table 3). Although it has been reported that photogenerated electrons are able to reduce nitrate and nitrite [63], as the conduction band electron density on TiO_2 was increased due to electrons migration from Cu_2O , the localised photogenerated electrons were able to reduce nitrate to NO_2^- ; N_2 or NH_4^+ in two, five and eight-electron reduction steps, respectively, (Eqs. (12)–(14)). It has also been demonstrated that photogenerated electrons could partake in the photocatalytic reduction of nitrate [19,21]. Similarly, the reduction could proceed via reduction of NO_2^- to NH_4^+ involving a six-electron transfer in the electron-dense conduction band of TiO_2 (Eq. (15)).

The photocatalytic reduction of nitrate in the presence of oxalic acid over $\text{Cu}_2\text{O}/\text{TiO}_2$, produced nitrogen, nitrite and ammonium as products. Higher Cu_2O loadings favoured rapid oxalate removal (Table 3) and this appeared to enhance ammonium selectivity

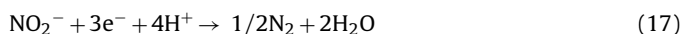
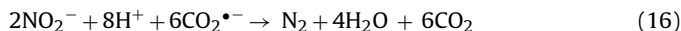
(Fig. 9c) suggesting that the reaction expressed by Eq. (10) may play a key role.

The process involved can be described by reactions expressed by Eqs. (9) and (13) but is largely dominated by reactions given in Eqs. (10) and (14), which implies that a larger amount of oxalic acid was consumed (Fig. 7a) compared with stoichiometric conversion and is consistent with the photodegradation profiles showing over-reduction (Fig. 6c). Along with ammonium, nitrite was also detected (Eq. (12)), but unlike ammonium, its concentration decreasing with the extent of reaction (Table 3 and Fig. 6c). This suggests that nitrite was readily formed and then subsequently converted to either nitrogen or ammonium (Eq. (11) and (15)). Over time, this ammonium contributed to an increase in solution pH along with the depletion of oxalic acid. Continued increases in ammonium could be due to either direct formation from nitrate or formed nitrite and was observed with increasing the Cu content in the photocatalyst composites. If the carbon dioxide anion radical ($\text{CO}_2\bullet^-$) was solely responsible for the reduction of NO_3^- to NH_4^+ , then each mole of nitrate would require 4 mol of oxalic acid (i.e., $4\text{C}_2\text{O}_4^{2-} \rightarrow 8\text{CO}_2\bullet^-$). However, the observed experimental data indicated that the least and highest effective oxalate-nitrate molar ratios are approximately 1.3 and 3.1, respectively and therefore, this reflects that $\text{CO}_2\bullet^-$ was not alone responsible for the reduction of nitrate. Hence, the reduction process also occurred via multi-electron transfer, as is more thermodynamically favourable than the single-electron reduction of nitrate [64]. On the other hand, multi-electron reaction requires H^+ ions, and consequently, pH is a key factor. In support of a mechanism involving multiple electron transfer, as all the reactions were carried out without adjustment of pH conditions, the reduction reactions proceeded progressively, but once the extent of deletion of oxalic acid was considerable, nitrate reduction ceased (Figure SI-2), which related to the unavailability of oxalic acid (hole scavenger) during the reaction environment. On the contrary, where oxalic acid not fully consumed thorough the course of the reaction, nitrate reduction was sustained until the end of the reaction time (Figure SI-3).





In support of the consequences of rapid consumption of oxalic acid on the selectivity for N₂, experiments conducted with 2.5% Cu₂O/TiO₂-AC photocatalysts, show a higher selectivity for N₂ than ammonium, even though conversion of nitrate was low. It is noted that the selectivity to ammonium was suppressed when the rate of consumption of oxalic acid was reduced (Figure SI- 3), which corresponds to Eq. (9) and (13). With the activated carbon containing composites, the reduction of nitrate to N₂ seems to be dominant under conditions where there is a gradual consumption of oxalic acid which also diminished the extent of reactions expressed by Eqs. (10), (11), (12), (14) and (15), as the amounts of ammonium and nitrite liberated were drastically reduced. These results suggest that by controlling the rate of consumption of oxalic acid, enhanced selectivity to N₂ could be achieved at reasonable nitrate conversion levels. It appears that higher selectivity to undesired products, particularly ammonium, was favoured by the rapid deletion of oxalic acid. Interestingly, in the reaction with 2.5% Cu₂O/TiO₂-20AC (Fig. 9c) no nitrite was detected, consistent with the rate of oxalic acid utilisation in the reaction environment influencing selectivity towards a particular reaction product(s). Furthermore, as there was no evolution of nitrite in the reaction carried out with 2.5% Cu₂O/TiO₂-20AC photocatalyst, it might be inferred that any nitrite formed during the reaction was then reduced by either CO₂•− since E°(NO₂−/N₂) = 1.45 V (Eq. (16)) [9] or/and by the created electron-dense conduction band of TiO₂ being the electron-populated site of Cu₂O/TiO₂ (Eq. (17)). This perhaps contributed to the formation of additional N₂, thus contributing to the highest observed N₂ selectivity of 78.4%, although nitrate conversion was relatively low (12.7%).



4. Conclusions

Cu₂O/TiO₂ and Cu₂O/TiO₂-AC photocatalyst composites were synthesised by an ethanol reduction method and subsequent characterisation by XRD, H₂-TPR and FTIR of adsorbed CO suggest that copper was present as Cu₂O. The 2.5% Cu₂O/TiO₂ sample (optimum Cu₂O loading) exhibited 57.6 and 99.8% removal of nitrate and oxalic acid, respectively, but favoured ammonium formation rather than nitrogen. Addition of AC to the mixed oxide composite reduced the rates of oxalic acid and nitrate degradation but also significantly decreased the selectivity to ammonium. A selectivity to nitrogen of ≈ 80% could be achieved at 20% nitrate conversion using 2.5% Cu₂O/TiO₂-20AC. Improved selectivity to nitrogen appeared to be attained in cases where the relative rate of oxalic acid was diminished.

Acknowledgements

This research supported by the Petroleum Technology Development Fund (PTDF) of Nigeria. We are grateful to Abubakar Tafawa Balewa University, Bauchi-Nigeria for the award of a studentship (to HA).

Appendix A. Supplementary data

Supplementary data associated with this article can be found, in the online version, at <http://dx.doi.org/10.1016/j.apcatb.2017.05.091>.

References

- [1] F.T. Wakida, D.N. Lerner, Water Res. 39 (2005) 3.
- [2] J. Hirayama, Y. Kamiya, ACS Catal. 4 (2014) 2207.
- [3] M. Saeed, M. Ilyas, M. Siddique, A. Ahmad, Arab. J. Sci. Eng. 38 (2013) 1739.
- [4] F.J. Beltrán, F.J. Rivas, R. Montero-de-Espinosa, Water Res. 39 (2005) 3553.
- [5] M. Shand, J.A. Anderson, Catal. Sci. Technol. 3 (2013) 879.
- [6] M.R. Hoffmann, S.T. Martin, W. Choi, D.W. Bahnemann, Chem. Rev. 95 (1995) 69.
- [7] W. Gao, R. Jin, J. Chen, X. Guan, H. Zeng, F. Zhang, N. Guan, Catal. Today 90 (2004) 331.
- [8] R. Jin, W. Gao, J. Chen, H. Zeng, F. Zhang, Z. Liu, N. Guan, J. Photochem. Photobiol. A 162 (2004) 585.
- [9] F. Zhang, R. Jin, J. Chen, C. Shao, W. Gao, L. Li, N. Guan, J. Catal. 232 (2005) 424.
- [10] Y. Li, F. Wasgestian, J. Photochem. Photobiol. A 112 (1998) 255.
- [11] J. Sá, C.A. Agüera, S. Gross, J.A. Anderson, Appl. Catal. B: Environ. 85 (2009) 192.
- [12] A. Kudo, K. Domé, M. Maruya, T. Onishi, Chem. Lett. 16 (1987) 1019.
- [13] K.T. Ranjit, B. Viswanathan, J. Photochem. Photobiol. A 107 (1997) 215.
- [14] K.T. Ranjit, B. Viswanathan, J. Photochem. Photobiol. A 108 (1997) 73.
- [15] B. Bems, F.C. Jentoft, R. Schlögl, Appl. Catal. B: Environ. 20 (1999) 155.
- [16] H. Kominami, T. Nakaseko, Y. Shimada, A. Furusho, H. Inoue, S.- Murakami, Y. Kera, B. Ohtani, Chem. Commun. (2005) 2933.
- [17] N. Wehbe, M. Jaafar, C. Guillard, J. Herrmann, S. Miachon, E. Puzenat, N. Guilhaume, Appl. Catal. A: Gen. 368 (2009) 1.
- [18] L. Li, Z. Xu, F. Liu, Y. Shao, J. Wang, H. Wan, S. Zheng, J. Photochem. Photobiol. A 212 (2010) 113.
- [19] H. Gekko, K. Hashimoto, H. Kominami, Phys. Chem. Chem. Phys. 14 (2012) 7965.
- [20] D.b. d. Luiz, S.L.F. Andersen, C. Berger, H.J. José, Moreira Regina de Fátima, Peralta Muniz, J. Photochem. Photobiol. A 246 (2012) 36.
- [21] K. Doudrick, T. Yang, K. Hristovski, P. Westerhoff, Appl. Catal. B: Environ. 136–137 (2013) 40.
- [22] J. Hirayama, H. Kondo, Y. Miura, R. Abe, Y. Kamiya, Catal. Commun. 20 (2012) 99.
- [23] J. Hirayama, R. Abe, Y. Kamiya, Appl. Catal. B: Environ. 144 (2014) 721.
- [24] J.A. Anderson, Catal. Today 181 (2012) 171.
- [25] V. Subramanian, E.E. Wolf, P.V. Kamat, J. Am. Chem. Soc. 126 (2004) 4943.
- [26] A.L. Linsebigler, G. Lu, J.T. Yates Jr., Chem. Rev. 95 (1995) 735.
- [27] I. Ganesh, P.P. Kumar, I. Annapoorna, J.M. Sulmeyer, M. Ramakrishna, N.Y. Heikal, G. Padmanabham, G. Sundararajan, Appl. Surf. Sci. 293 (2014) 229.
- [28] J.A. Seabold, K. Shankar, R.H.T. Wilke, M. Paulose, O.K. Varghese, C.A. Grimes, K.- Choi, Chem. Mater. 20 (2008) 5266.
- [29] H. He, P. Xiao, M. Zhou, Y. Zhang, Q. Lou, X. Dong, Int. J. Hydrogen Energy 37 (2012) 4967.
- [30] Y. Li, B. Wang, S. Liu, X. Duan, Z. Hu, Appl. Surf. Sci. 324 (2015) 736.
- [31] D.M. Tobaldi, N. Rozman, M. Leoni, M.P. Seabra, A.S. Škapin, R.C. Pullar, J.A. Labrincha, J. Phys. Chem. C (2015).
- [32] L. Yang, S. Luo, Y. Li, Y. Xiao, Q. Kang, Q. Cai, Environ. Sci. Technol. 44 (2010) 7641.
- [33] G. Jiang, R. Wang, H. Jin, Y. Wang, X. Sun, S. Wang, T. Wang, Powder Technol. 212 (2011) 284.
- [34] Y. Bessekhouad, D. Robert, J.- Weber, Catal. Today 101 (2005) 315.
- [35] M. Lei, N. Wang, L. Zhu, Q. Zhou, G. Nie, H. Tang, Appl. Catal. B: Environ. 182 (2016) 414.
- [36] K. Lalitha, G. Sadanandam, V.D. Kumari, M. Subrahmanyam, B. Sreedhar, N.Y. Heikal, J. Phys. Chem. C 114 (2010) 22181.
- [37] Z. Wang, Y. Liu, D.J. Martin, W. Wang, J. Tang, W. Huang, Phys. Chem. Chem. Phys. 15 (2013) 14956.
- [38] H. Yu, J. Yu, S. Liu, S. Mann, Chem. Mater. 19 (2007) 4327.
- [39] T. Lim, P. Yap, M. Srinivasan, A.G. Fane, Crit. Rev. Environ. Sci. Technol. 41 (2011) 1173.
- [40] M. Inagaki, Y. Hirose, T. Matsunaga, T. Tsumura, M. Toyoda, Carbon 41 (2003) 2619.
- [41] B. Tryba, A.W. Morawski, M. Inagaki, Appl. Catal. B: Environ. 41 (2003) 427.
- [42] C.H. Ao, S.C. Lee, Appl. Catal. B: Environ. 44 (2003) 191.
- [43] J. Matos, J. Laine, J. Herrmann, Appl. Catal. B: Environ. 18 (1998) 281.
- [44] L.F. Velasco, J.B. Parra, C.O. Ania, Appl. Surf. Sci. 256 (2010) 5254.
- [45] D.A. Shirley, Phys. Rev. B 5 (1972) 4709.
- [46] W.T. Bolteeter, C.J. Bushman, P.W. Tidwell, Anal. Chem. 33 (1961) 592.
- [47] M. Ouzzine, A.J. Romero-Anaya, M.A. Lillo-Ródenas, A. Linares-Solano, Carbon 67 (2014) 104.
- [48] S. Zhu, S. Liang, Y. Tong, X. An, J. Long, X. Fu, X. Wang, Phys. Chem. Chem. Phys. 17 (2015) 9761.
- [49] F. Coloma, B. Bachiller-Baeza, C.H. Rochester, J.A. Anderson, Phys. Chem. Chem. Phys. 3 (2001) 4817.
- [50] F. Bocuzzi, A. Chiorino, G. Martra, M. Gargano, N. Ravasio, B. Carrozzini, J. Catal. 165 (1997) 129.

- [51] G. Wu, N. Guan, L. Li, *Catal. Sci. Technol.* 1 (2011) 601.
- [52] L. Liu, C. Zhao, Y. Li, *J. Phys. Chem. C* 116 (2012) 7904.
- [53] C. Prestipino, L. Regli, J.G. Vitillo, F. Bonino, A. Damin, C. Lamberti, A. Zecchina, P.L. Solari, K.O. Kongshaug, S. Bordiga, *Chem. Mater.* 18 (2006) 1337.
- [54] Z. Wu, H. Zhu, Z. Qin, H. Wang, L. Huang, J. Wang, *Appl. Catal. B: Environ.* 98 (2010) 204.
- [55] C. Tu, S. Cheng, *ACS Sustain. Chem. Eng.* 2 (2014) 629.
- [56] S. Yilmaz, E. McGlynn, E. Bacaksiz, Ş. Özcan, D. Byrne, M.O. Henry, R. Chellappan, *J. Appl. Phys.* 111 (2012) 013903.
- [57] H. Kominami, A. Furusho, S. Murakami, H. Inoue, Y. Kera, B. Ohtani, *Catal. Lett.* 76 (2001) 31.
- [58] A. Paracchino, V. Laporte, K. Sivula, M. Grätzel, E. Thimsen, *Nat. Mater.* 10 (2011) 456.
- [59] U.I. Gaya, A.H. Abdullah, *J. Photochem. Photobiol. C: Photochem. Rev.* 9 (2008) 1.
- [60] M.A. Rauf, M.A. Meetani, S. Hisaindee, *Desalination* 276 (2011) 13.
- [61] B. Gao, P.S. Yap, T.M. Lim, T. Lim, *Chem. Eng. J.* 171 (2011) 1098–1107.
- [62] W. Wei, C. Yu, Q. Zhao, X. Qian, G. Li, Y. Wan, *Appl. Catal. B: Environ.* 146 (2014) 151.
- [63] H. Ren, S. Jia, J. Zou, S. Wu, X. Han, *Appl. Catal. B: Environ.* 176–177 (2015) 53.
- [64] A.R. Cook, N. Dimitrijevic, B.W. Dreyfus, D. Meisel, L.A. Curtiss, D.M. Camaioli, *J. Phys. Chem. A* 105 (2001) 3658.